Available online at www.sciencedirect.com
SCIENCE DIRECT
Cement and Concrete Research 36 (2006) 1379–1388
Cement and Concrete Research

Stability of ancient masonry towers: Moisture diffusion, carbonation and size effect

Daniele Ferretti [a], Zdeněk P. Bažant [b,*]

[a] University of Parma, Parco Area delle Scienze 181/A, 43100 Parma, Italy
[b] Northwestern University, 2145 Sheridan Road, CEE, Evanston, Illinois 60208, USA

Received 23 December 2004; accepted 16 March 2006

Abstract

Moisture diffusion and carbonation influence the behavior of multiple-leaf ancient masonry walls, producing during centuries a redistribution of stresses from the core of lime mortar concrete to the external cladding of stiff masonry. This is likely one of the causes of long-time damage of some ancient masonry towers. With these motivations, coupled processes of moisture diffusion, carbon dioxide diffusion and carbonation reaction are analyzed numerically. Due to the absence of models and data for lime mortar, one of the simplest models proposed for Portland cement concrete is adapted for this purpose. The results reveal the time scales of the processes involved and their dependence on wall thickness (size). It is found that the temporal scale is set mainly by diffusion of moisture trough the massive concrete wall and is only slightly modified by carbonation. Moisture evolution in time is needed for stress analysis that is relegated to a subsequent paper.

Keywords: C Carbonation; A Humidity; C Diffusion; C Long-term performance; Tower

1. Introduction

In 1989, eight centuries after its construction, the Civic Tower of Pavia (Fig. 1a), Italy, collapsed suddenly, with imperceptible warning signals . This dramatic event was only the last in a series of failures of masonry towers built in Europe between the 11th and 14th centuries. Other examples are the collapse in 1902 of the Campanile in San Marco Square in Venice (whose present day structure is a replica of its predecessor [1]) and the collapse of the bell tower of the church of St. Magdalena in Goch (Germany) in 1992. In addition, there are plenty of ancient towers that are seriously damaged. After many centuries of uneventful existence, their surfaces are now seen to develop systems of growing vertical cracks propagating through mortar joints and also cutting through the bricks of masonry walls. This problem affects towers built with solid brick walls (e.g., Campanile in San Marco Square, Monza Cathedral, Torrazzo in Cremona), as well as multiple-leaf walls (e.g., Civic Tower of Pavia, Ravenna Tower, Tower of St. Giustina in Padua).

Multiple-leaf walls consist of two external layers (claddings) of good coursed masonry 150 to 250 mm thick, filled up by 1 to 4 m of a particular ancient concrete consisting of lime mortar, river gravels and recycled bricks (Fig. 1b,c). Ancient lime concrete is different from modern Portland cement concrete. Sometimes, the rubble is disordered and loose. In other cases, it consists of ordered layers of bricks and gravel alternating with thick layers of lime mortar. Fissures in these walls or the tendency of the external layers to spall off were discussed by some authors (e.g. [2–5]). They observed that, for Pavia Tower as well as most others, the foundation settlements, overloads, lightning effects and chemically induced decay must be excluded as the causes of cracking. Also, the average stress due to the weight of these towers is high but generally not critical. For instance, in the case of the Civic Tower of Pavia, which serves here as a paradigm, the average vertical normal stress at the base was only 1.1 MPa, while the average uniaxial compressive strength of the core was measured to be about 3.0 MPa [5]. Three-dimensional

* Corresponding author.
E-mail addresses: daniele.ferretti@unipr.it (D. Ferretti), z-bazant@northwestern.edu (Z.P. Bažant).

0008-8846/$ - see front matter © 2006 Elsevier Ltd. All rights reserved.
doi:10.1016/j.cemconres.2006.03.013

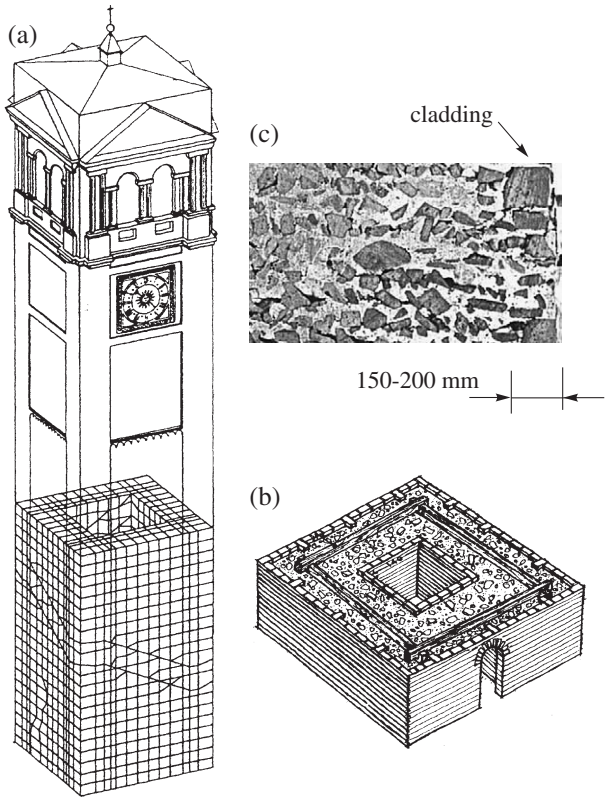

Fig. 1. Ancient tower: (a) geometry and finite element mesh of the Civic Tower of Pavia, Italy (after [5]); (b) typical cross section; (c) photo of the masonry wall of the Civic Tower of Pavia.

nonlinear finite element analyses were conducted (Fig. 1a) and showed that a severe stress concentration exhausting the compression strength existed at the base of the staircase, near the entrance to the tower [5]. However, although the ruins confirm that stress concentration might have triggered local failure, neither the overall collapse after centuries nor the development of crack patterns in the cladding many years before the collapse [5] could be explained by these finite element analyses.

To explain failure, it is necessary to take into account the effect of time. Specimens taken from Pavia ruins and from others ancient walls were tested under constant compression stresses for long time [6,7]. The compression strain at constant stress equal to 40–50% of compressive strength increased in time and was accompanied by growth of splitting microcracks. The strain–time curve at constant stress had the form of a creep curve with secondary and tertiary creep phases [7], which must be explained by damage microcracks growth (and must be sensitive to the lateral confining stress). Researchers modelled this time-dependent behavior by a viscoelastic-damage law [8] and used it for finite element analyses. Computations showed that the damage zones produced by stresses concentration propagate in time up to failure of the structure [9]. During centuries, this damage growth was probably intensified by fatigue effects due to cyclic stresses produced by wind and bell ringing. Up to depth $d<\sqrt{6ct_p}$ (Eq. (7) in [10], c=thermal diffusivity, about 1 mm^2 s^{-1}, t_p=fluctuation period), which is 0.7 m for t_p=1 day and all wall thickness for t_p=1 year, the material also suffers cyclic stresses due to temperature fluctuations in the environment, different at various sides [11].

Most importantly, in massive walls, especially multiple-leaf walls, the stress distribution is nonuniform and evolves in time. Time effects arise from creep, drying, and carbonation. For this problem, a comprehensive mathematical model is still missing. Its development is the objective of this study.

2. Nature of long-term processes involved and failure scenario

The nonuniform stresses caused in multiple-leaf walls by shrinkage, creep and carbonation evoke similarities with modern multi-layer masonry walls, in which the effects of moisture diffusion, drying and creep are known to cause microcracks due to redistribution of stresses among the different layers [12]. Such phenomena must be expected also in the walls of ancient towers. The cladding, consisting of stone or brick masonry, creeps and shrinks very little. For this reason, shrinkage and creep of the core (basic creep plus drying creep) must cause gradual transfer of stresses from the core to the cladding. Further stress transfer in the horizontal cross section can also be caused by volume changes due to carbonation of lime concrete, which slowly propagates from the outside to the inside of the core. Why should these processes take centuries?

The temporal scale is set by the diffusion of moisture through the massive wall, and is somewhat modified by carbonation. The half-time of diffusion processes is known to be proportional to the square of thickness. The ancient concrete appears to have roughly similar diffusion properties as modern low-strength concrete and, for a 0.15 m thick wall of such concrete, the drying half-time is about 2 years. So, for 2.80 m thick wall of ancient concrete, the half-time is expected to be about $(2.80/0.15)^2\times 2\approx 700$ years. This is confirmed by the evidence that very thick ancient walls built centuries ago are still far from completely dry and carbonated.

As hypothesized by Bažant and Ferretti [13], during the initial stage of drying, concrete near the exterior cladding shrinks and undergoes additional creep due to drying. This causes tensile stress increments, which must be balanced by compressive stress increase in the central portion of the wall. The stresses in concrete, though not those in the cladding, relax due to creep. During the terminal stage of drying, the central portion of the wall shrinks and additionally contracts due to drying creep. This reduces compressive stresses in the central portion, which must be balanced by an increase of compressive stresses both in the cladding and in the concrete near the cladding. The resulting increase of compressive stress may cause secondary creep, tertiary creep and compression failure of the surface layer of the wall, which can take the form of either crushing of the cladding with the adjacent concrete, or delamination buckling of the cladding.

In either case, the compression failure would not be simultaneous because compression failure is not plastic but softening so the failure cannot be simultaneous, as typical of plasticity, but must localize and propagate transversely. Transverse propagation is governed by fracture mechanics, i.e. by the energy release rate. As is well known, this rate may be calculated for constant load or

constant displacement, both of which give the same result (e.g. [14]). Even though the vertical load is constant, calculation is simpler for constant vertical displacement at remote cross sections of tower. In that case, the stresses in the zones of the flanks of the propagating compression failure get reduced (at constant displacement), and so the strain energy is released from these zones and must get dissipated somewhere. It gets dissipated by flowing into the front of the failed layer and driving its propagation. Owing to the large dimensions of the wall, the result must be a size effect—i.e., the apparent, or nominal, strength of the masonry cladding on a large scale must be less than that measured on laboratory specimens [14–16]. The length of the failed layer at collapse may reasonably be assumed to be proportional to the cross section dimension of the wall. The cause of the size effect is the fact that the volume of the partially unloaded zone on the flanks of the failed layer, and thus also the energy released from that zone, grow quadratically with the length of the failed layer, while the energy consumed by fracturing at the front of the failed layer grows linearly. Obviously, energy could not be in balance if the average vertical stress before failure were the same for long and short failed layers [13,17].

To demonstrate the possibility of the scenario just outlined, humidity diffusion and carbonation are modelled first. Two subsequent papers will analyze interaction with creep and fracture.

3. Mechanism of humidity diffusion and its coupling with carbonation

The diffusion of humidity in a concrete-like material is a very slow phenomenon. It is well known (e.g. [18,19]) that even the standard test cylinder of concrete takes years to dry to a uniform pore humidity. Therefore, it is not surprising that drying of a lime concrete wall several meters thick necessitates centuries.

During this long period, humidity diffusion interacts with carbonation of lime, which is also a very slow phenomenon. Carbonation is activated by diffusion of carbon dioxide from the environment into partially dried concrete pores where the lime and carbon dioxide reacts while dissolved in the pore water. Besides, a decrease of water content in the pores slows the diffusion down. Therefore, the water content and diffusion play an important role in the diffusion of carbon dioxide in lime mortar and in the consequent carbonation. Vice versa, carbonation reduces porosity, which retards moisture diffusion.

Although the reaction kinetics of carbonation is rather complex, it can be simply treated as a two-stage process [20,21]. In the first stage, CO_2 diffuses from the atmosphere into the partially dried capillary pores and combines with water to form carbonic acid:

$$CO_2 + H_2O \rightleftharpoons H_2CO_3 \tag{1}$$

Then, calcium hydroxide $Ca(OH)_2$ (also known as portlandite) dissolves in the pore water and reacts with dissolved CO_2 to form calcium carbonate (calcite)

$$Ca(OH)_2 + H_2CO_3 \rightarrow CaCO_3 + 2H_2O \tag{2}$$

This simplified reaction ignores the formation of other precipitates. For example, in limes of dolomitic origin, together with carbonation of $Ca(OH)_2$, also carbonation of $Mg(OH)_2$ may occur. In urban environment, also sulfatation could be very important, since it could be the origin of damage and collapse. However, in the case of Pavia Tower, chemical tests proved that these processes were negligible [5].

To describe the physicochemical process of carbonation, mathematical models were proposed for lime mortar [20,22], as well as Portland cement concrete [23–31], in which similar reactions occur because of presence of calcium hydroxide in the cement paste. Because of this similarity, carbonation of lime mortar was often studied in the past to investigate carbonation of Portland cement mortar and vice versa. For this reason, some authors [20,32] suggest using the same mathematical models for carbonation of both materials. Of course, physicochemical characteristics, such as porosity and portlandite concentration, should be recalibrated with tests.

The present study adopts the simple model of Saetta, Schrefler and Vitaliani [26–28]. To calibrate the parameters of the model, only a few useful tests in the sense of [28] are available for lime mortar (e.g. [33]), whereas no data seem to be available for ancient lime concrete. For this reason, when data are missing, we assume parameters typical of low strength Portland cement concrete, while being aware of the approximate nature of the results.

3.1. Carbonation of lime

According to the adopted model, the rate of relative concentration of carbonate, $\mathcal{R} = [CaCO_3]/[CaCO_3]_{max}$, is governed by the equation [23,26,28]

$$\frac{\partial \mathcal{R}}{\partial t} = \alpha_1 f_1(h) f_2(c) f_3(\mathcal{R}) f_4(T) \tag{3}$$

where the factor $\alpha_1 f_4(T) \approx 0.019$ day^{-1} takes into account the kinetics of the chemical reaction, h represents the relative humidity in the pores, c = concentration of CO_2, T = absolute temperature and $[CaCO_3]_{max}$ = maximum mass concentration of calcium carbonate (kg m^{-3} of concrete).

The kinetics of the chemical reaction in ancient lime mortar is different from the recent commercial lime mortar. Because of the ageing during several years storage of slaked lime under water, portlandite crystals were smaller and carbonation was faster [34]. This should be reflected in some increase of the coefficient α_1. However, this question is not important here because carbonation is much faster than diffusion of CO_2 in a thick wall [22].

The effect of relative humidity h is governed by the function

$$f_1(h) = \begin{cases} 0 & 0 \le h < 0.5 \\ 2.5(h-0.5) & 0.5 \le h < 0.9 \\ 1 & 0.9 \le h < 1 \end{cases} \tag{4}$$

which vanishes (i.e. the reaction is stopped) when the water available in the pores is not sufficient for the dissolution of lime and carbon dioxide [35].

The effect on concentration of carbon dioxide, c, is taken into account by the factor $f_2(c) = c/c_{max}$ where $c_{max} = 0.035\%$ is the assumed maximum volume concentration of carbon dioxide in

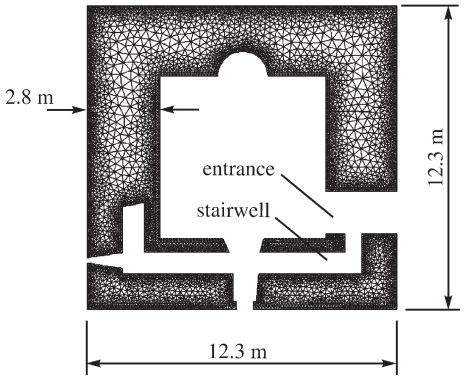

Fig. 2. Finite element mesh of a horizontal cross section of Pavia Tower (at the height of 5 m).

the air. Finally, the influence of the degree of carbonation $\mathcal{R}$ is introduced by means of coefficient $f_3(\mathcal{R}) = 1-\mathcal{R}$ that vanishes when the reaction is complete.

The massive wall is assumed to be at constant uniform temperature equal to the annual average of $T=284$ K (=11 °C) in Pavia. Also, the temperature variations produced by exothermic reactions during setting, hardening and ageing are disregarded at the moment.

3.2. Humidity diffusion

The moisture diffusion from the core of the tower to the external environment is described in terms of relative humidity h using the semi-theoretical nonlinear model proposed in [18]. This model was generalized in [26] for coupling with carbonation caused by moisture liberation due to growth of $\mathcal{R}$

$$\frac{\partial h}{\partial t} = \nabla\cdot(C\nabla h) + \frac{\partial h_s}{\partial t} + \alpha_2\frac{\partial \mathcal{R}}{\partial t} \tag{5}$$

where C is the diffusivity, h_s is the self-desiccation term (which here represents the effects of consumption or liberation of water by the other chemical reactions) and $\alpha_2 \approx 0.0017$ describes the effect on pore humidity h of water liberated during carbonation. Diffusivity C is assumed in the form

$$C = C_0 F_1{}^*(h) F_2(T) F_3(t_e) F_4(\mathcal{R}) \tag{6}$$

where C_0 is the diffusivity at saturation in standard conditions (at the age of 28 days and at room temperature, $T=T_0=296$ K). The factors

$$F_1{}^*(h) = \alpha_0 + \frac{1-\alpha_0}{1+\left(\frac{1-h}{1-h_c}\right)^n} \tag{7a}$$

$$F_2(T) = \exp\left(\frac{Qh}{RT_0} - \frac{Qh}{RT}\right) \tag{7b}$$

$$F_3(t_e) = \chi + (1-\chi)\left(\frac{28}{t_e}\right)^{0.5} \tag{7c}$$

$$t_e = \int_0^t \beta_h \mathrm{d}t = \int_0^t [1+(5-5h)^4]^{-1}\mathrm{d}t \tag{7d}$$

are semi-empirical expressions that take into account the effects of humidity h, temperature T and equivalent hydration time t_e [18]. Similarly to a low strength Portland cement concrete, it is assumed that $C_0 \approx 10$ mm^2 day^{-1}, $\alpha_0=0.05$, $h_c=0.75$, $n=6$, $Qh/R=2700$ K and $\chi \approx 0.8$.

The microstructure of lime mortar changes during carbonation. The volume fraction of small diameter pores increases, whereas the large pores are filled by the expanding microcrystalline or amorphous calcium carbonate. This produces a reduction of total porosity [21,25,35], which is described by the factor $F_4(\mathcal{R}) = 1-\zeta\mathcal{R}$ where $\zeta \approx 0.3$ [27].

3.3. Diffusion of carbon dioxide

Diffusion of carbon dioxide into concrete-like materials can be described in terms of Fick's law

$$\frac{\partial c}{\partial t} = \nabla\cdot(D_c\nabla c) - \alpha_3\frac{\partial \mathcal{R}}{\partial t} \tag{8}$$

in which the last term is the sink term accounting for the consumption of carbon dioxide during carbonation [26]; $c=[CO_2]$, $\alpha_3 \approx 0.40$ and D_c is the diffusivity of CO_2 in concrete, which may be expressed as

$$D_c = D_{c,0} F_1(h) F_2(T) F_3(t_e) F_4(\mathcal{R}). \tag{9}$$

Here $F_1(h)=(1-h)^{2.5}$, while the other factors are the same as in Eq. (7a) (7b) (7c) and (7d). Coefficient $F_1(h)$ reflects the retarding of CO_2 diffusion with increasing humidity. When water fills the pores, CO_2 must first dissolve and then diffuse to a liquid phase rather than gas to penetrate deeper [35]. In this case, diffusivity D_c reduces by several orders of magnitude [24,33,35]. In Portland cement, concrete diffusivity of carbon dioxide, $D_{c,0}$, at normal conditions ($t=28$ days and $T=296$ K) is strongly influenced by the water–cement ratio [25,27]; for a poor concrete with high water–cement ratio $D_{c,0} \approx 2400$ mm^2 day^{-1}. The presence of aggregates does not affect appreciably the value of effective diffusivity because the occurrence of cracks between cement paste and aggregates seems to compensate for the lack of porosity of the aggregates [24]. The same value is adopted for our ancient concrete.

The multifactor law (9) is debatable. For instance, [20,29,22] adopt more complex multiplying factors. Nevertheless, for lack of experimental data on ancient lime mortars, the

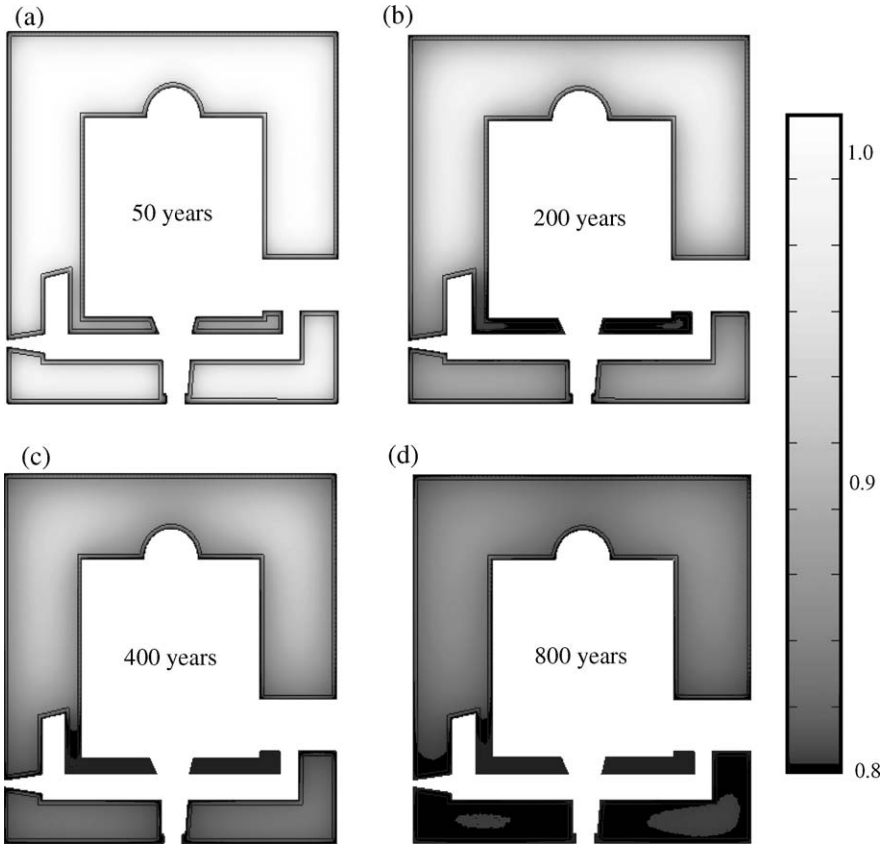

Fig. 3. Finite element map of relative pore humidity h: (a) $t=50$ years, (b) $t=200$ years, (c) $t=400$ years, (d) $t=800$ years.

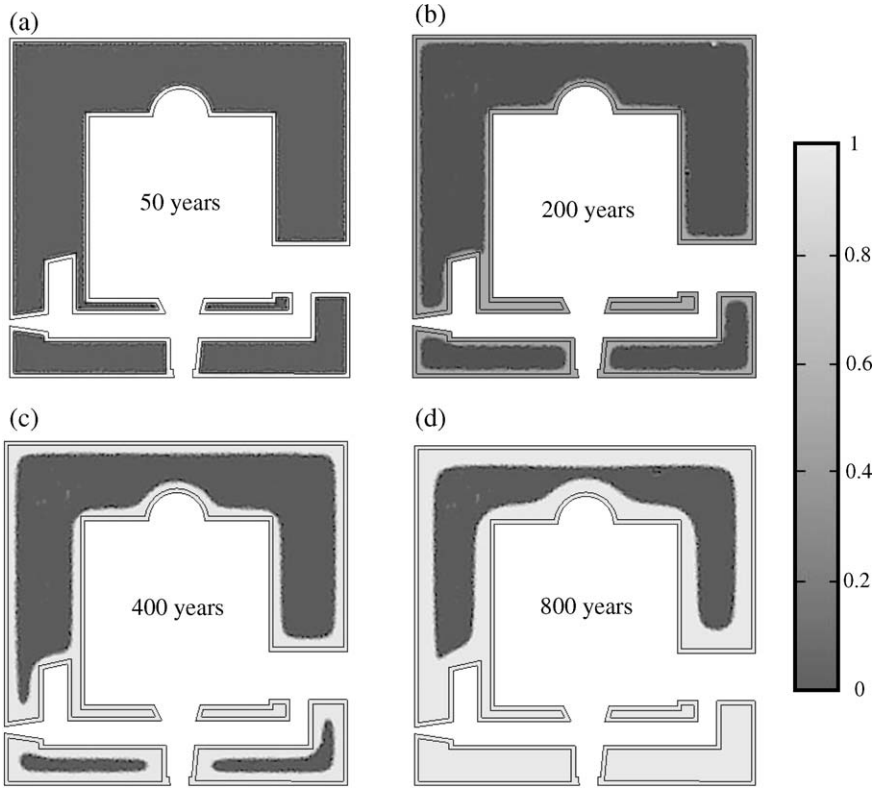

Fig. 4. Finite element map of relative carbonation $\mathcal{R}$: (a) $t=50$ years, (b) $t=200$ years, (c) $t=400$ years, (d) $t=800$ years.

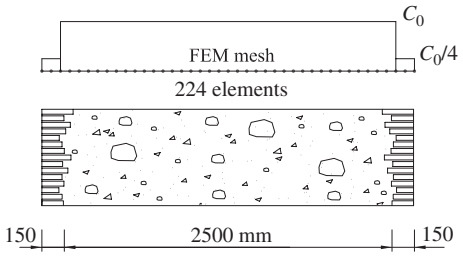

Fig. 5. Cross section of a wall of Pavia Tower: finite element mesh for the analysis in one dimension.

model proposed in [26–28] is used here, for the sake of simplicity.

4. Numerical solution via finite element method

To study diffusion in a horizontal cross section of the tower, the system of partial differential Eqs. (3), (5) and (8) may be written in matrix form as

$$\begin{bmatrix} 1 & 0 & 0 \\ -\alpha_2 & 1 & 0 \\ \alpha_3 & 0 & 1 \end{bmatrix} \frac{\partial}{\partial t} \begin{bmatrix} \mathcal{R} \\ h \\ c \end{bmatrix} - \nabla \cdot \begin{bmatrix} 0 & 0 & 0 \\ 0 & C & 0 \\ 0 & 0 & D_c \end{bmatrix} \nabla \begin{bmatrix} \mathcal{R} \\ h \\ c \end{bmatrix} = \begin{bmatrix} \alpha_1 f_1 f_2 f_3 \\ 0 \\ 0 \end{bmatrix} \tag{10}$$

or in compact form

$$\mathbf{d}_a \frac{\partial \mathbf{u}}{\partial t} - \nabla \cdot \mathbf{c} \nabla \mathbf{u} = \mathbf{f} \text{ in } \Omega(x,y). \tag{11}$$

The Dirichlet and Neumann boundary conditions are

$$\underline{\mathbf{n}} \cdot (\mathbf{c} \nabla \mathbf{u}) + \mathbf{q}\mathbf{u} = \mathbf{g} - \mathbf{h}^T \boldsymbol{\lambda} \text{ on } \partial\Omega \tag{12}$$

$$\mathbf{h}\mathbf{u} = \mathbf{r} \text{ on } \partial\Omega \tag{13}$$

where $\mathbf{u} = [\mathcal{R}, h, c]^T, \Omega(x,y)$ represents the two-dimensional domain of boundary, $\partial\Omega$, and $\underline{\mathbf{n}}$ is its outward unit normal. The solution is obtained numerically by finite elements [27,36]. The initial boundary value problems (11) (12) and (13) is reduced to its weak form. Then, the problem is discretized by projecting the weak form onto a finite-dimensional function space, which is a set of linear shape functions on a triangularization of Ω. This leads to the following non-linear system of coupled ordinary differential equations in time:

$$\begin{bmatrix} \mathbf{D}_a & 0 \\ 0 & 0 \end{bmatrix} \begin{bmatrix} \frac{d\mathbf{U}}{dt} \\ 0 \end{bmatrix} + \begin{bmatrix} \mathbf{C}+\mathbf{Q} & \mathbf{H}^T \\ \mathbf{H} & 0 \end{bmatrix} \begin{bmatrix} \mathbf{U} \\ \boldsymbol{\Lambda} \end{bmatrix} \begin{bmatrix} \mathbf{F}+\mathbf{G} \\ \mathbf{R} \end{bmatrix} \tag{14}$$

where $\mathbf{U}$ is the discrete representation of $\mathbf{u}$, $\boldsymbol{\Lambda}$ are the Lagrange multipliers, and $\mathbf{D}_a$, $\mathbf{C}$, $\mathbf{Q}$, $\mathbf{H}$, $\mathbf{F}$, $\mathbf{G}$ and $\mathbf{R}$ are the matrices corresponding to $\mathbf{d}_a$, $\mathbf{c}$, $\mathbf{q}$, $\mathbf{h}$, $\mathbf{f}$, $\boldsymbol{\lambda}$ and $\mathbf{r}$, respectively. For their detailed expressions, see [27].

The system of nonlinear ordinary differential equations is diffusion-dominated (i.e. behaves similarly to heat diffusion) and involves components that decay at widely different rates. For this reason, it can be stiff and the classical explicit numerical methods of integration in time can lead to inaccurate results if the time steps are not small enough. For this reason, a very stable time integration scheme based on a backward difference formula of order two is adopted [37]. The method is implicit and uses the modified Newton-Raphson iterative algorithm to solve the non-linear algebraic equations.

5. An example: the case history of Pavia Tower

The proposed model is used to analyze the horizontal cross section of Pavia Tower (at a height of 5 m), as depicted in Fig. 2. The figure also shows triangular mesh used (with 10,328 elements and 5644 nodes). The mesh is refined near the openings, such as windows and staircase.

The behavior of the zones of the tower near the openings is three-dimensional. For this reason, the present two-dimensional analysis should be considered only as an approximation of the overall behavior or as a benchmark to check the validity of hypotheses. Anyway, because the diffusion properties of ancient lime mortar have scarcely been investigated, a more sophisticated analysis could hardly be more informative.

In the cladding, moisture permeates predominantly through the joints, whose permeability and diffusivity C and D_c are assumed to be the same as those of lime concrete. Thus, the

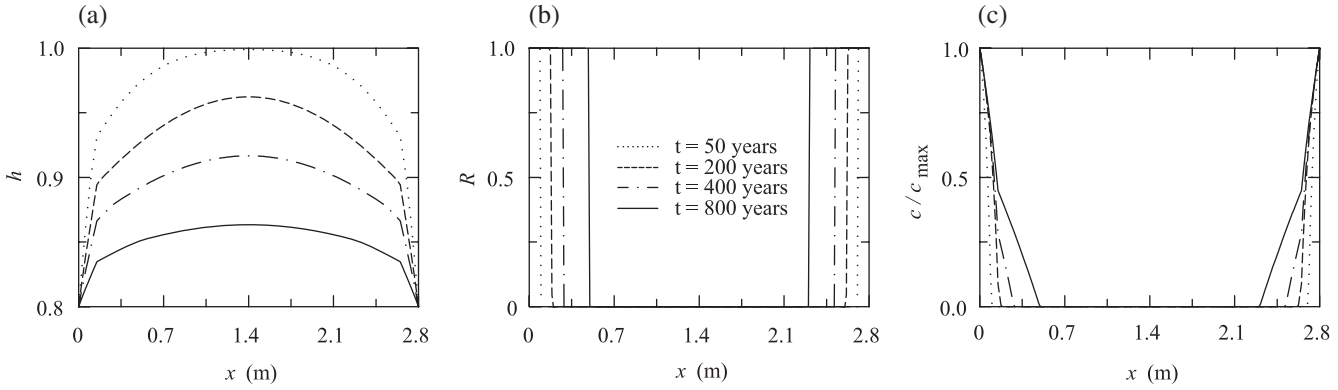

Fig. 6. Profiles after t=50, 200, 400, 800 years: (a) relative pore humidity h, (b) relative carbonation $\mathcal{R}$, (c) relative carbon dioxide concentration c/c_{max}.

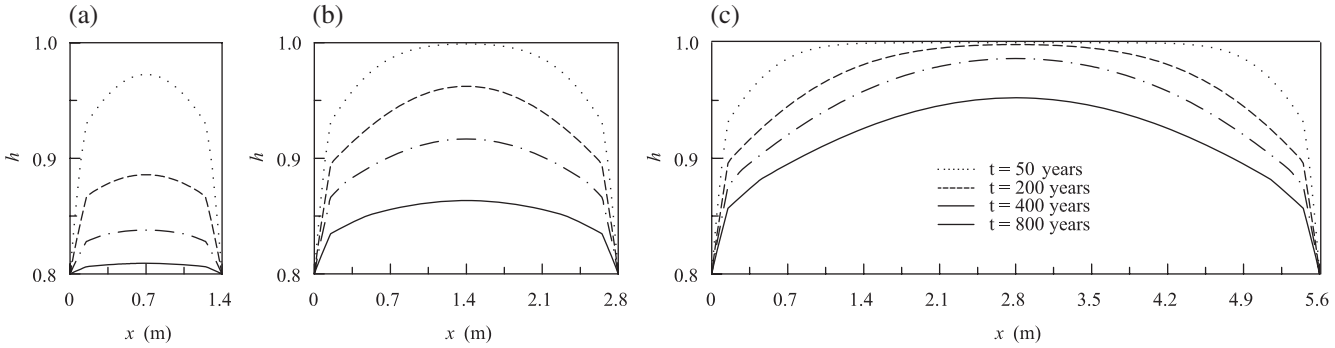

Fig. 7. Relative pore humidity profiles for walls of different thickness: (a) $D=1.4$ m, (b) $D=2.8$ m, (c) $D=5.6$ m.

effective diffusivity in the cladding layer is obtained by reducing the diffusivity of lime concrete in proportion to the cross section area fraction of the joints, which is about 1/4. The three-dimensional perturbation of the flow right beneath the cladding is neglected. Also, the moisture flow from the mortar joints to the bricks, which began right after the bricks were laid, and the subsequent reverse moisture flow from the bricks to the mortar [38] are disregarded.

The behavior is complicated by re-wetting of the cladding caused by rain. As pointed out in [29], rain and seasonal fluctuations of environmental relative humidity certainly affect the time evolution of moisture flow and, consequently, also the carbonation depth. Some authors state that in small specimens not sheltered from rain, drying is interrupted by rainy periods and capillarity suction takes up quickly the amount of water lost by drying [39]. In huge structures, this is impossible since it would imply uncarbonated walls. Rewetting seems also responsible for the formation of a thin layer of recarbonated material, which is very compact and poorly permeable [5]. In Pavia, environmental humidity is high and almost constant throughout the year. Fitting relative humidity data we have $\mathrm{RH}(t)=80\%+7\%\cos(2\pi t)$, with time t in years.

The concentration of CO_2 in the air, c_{env}, is about 0.035%. On the boundary $(x,y)\in\partial\Omega$, which is in contact with the environment, $h(x,y,t)=\mathrm{RH}(t)$, $c(x,y,t)=c_{\mathrm{env}}$, and $\mathcal{R}(x,y,t)=1$. The initial conditions at time $t=t_0$ and (x,y) are $h(x,y,t_0)=1.0$, $c(x,y,t_0)=0$ and $\mathcal{R}(x,y,t_0)=0$.

The numerical solution of Eqs. (11) (12) and (13) is represented in Fig. 3 in the form of constant pore humidity contours at times $t=50$, 200, 400 and 800 years after casting, the last being the time of failure. Fig. 3 confirms that the pore humidity field is not uniform and evolves for many centuries. Note that, in the thin walls, an approximately uniform humidity is reached within a few centuries (Fig. 3). Carbonation proceeds at any time at the advancing front separating a carbonated region (light gray in Fig. 4) from the rest, in which carbonation has not started yet (dark gray in Fig. 4). The thickness of the surface layer of carbonated lime mortar after eight centuries depends on the thickness of the walls; the thin walls are completely carbonated, whereas the massive walls are still carbonating. The nonuniformity of carbonation (Fig. 4) doubtless causes a nonuniformity of mechanical properties [40]. To illuminate the effect of the wall size, it is instructive to conduct a one-dimensional analysis.

6. Effect of size on diffusion phenomena

The procedure described in the previous paragraphs is now used for one-dimensional analysis of diffusion across the wall near the base of Pavia Tower. The wall has the thickness of $D=2.8$ m and is lined by good coursed masonry cladding of thickness $d=0.15$ m (Fig. 5). Eq. (3) is now specialized in one-dimension and is solved in space and time by finite elements, following the procedure already described for two dimensions. In particular, time interval $[t_0,t_f]$ is divided into discrete times t_r ($r=1, 2, \ldots, N$), with uniform steps $\Delta t=t_{r+1}-t_r$. The wall thickness, D, is subdivided into finite elements with Lagrange quadratic shape functions. Fig. 5 shows the nodes of coordinates x_i ($i=1, 2, \ldots, n$) spaced at constant intervals $\Delta x=x_{i+1}-x_i=$

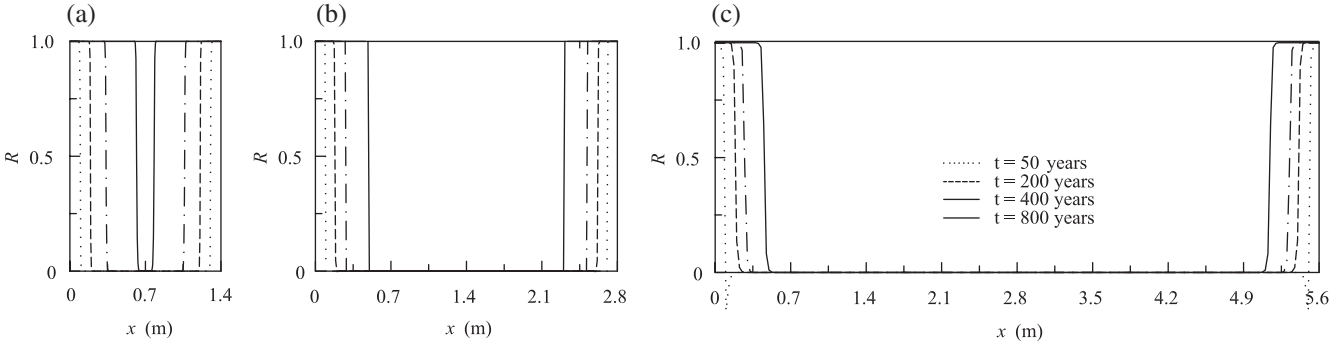

Fig. 8. Carbonation profiles of walls of different thickness: (a) $D=1.4$ m, (b) $D=2.8$ m, (c) $D=5.6$ m.

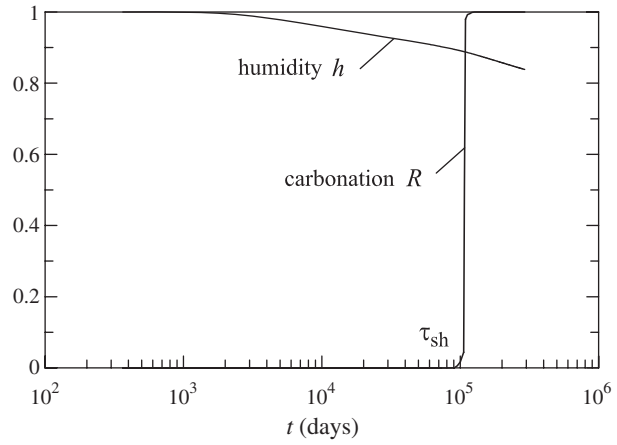

Fig. 9. Time curves (at point $x=0.4$ m) for relative carbonation $\mathcal{R}$ and relative pore humidity h.

12.5 mm. For the nodes in contact with the environment, the boundary conditions are $h(0,t)=h(D,t)=\mathrm{RH}(t)$, $c(0,t)=c(D,t)=0.035\%$. This corresponds to complete carbonation of the surface, i.e. $\mathcal{R}(0,t)=\mathcal{R}(D,t)=1$. The initial conditions at time $t=t_0$ are $h(x,t_0)=1.0$, $\mathcal{R}(x,t_0)=0$ and $c(x,t_0)=0\ \forall x\in[0,D]$.

The materials parameters are the same as previously considered for two dimensions. The effects of temperature fluctuations on moisture diffusion and carbonation are again neglected.

The results for the times of 50, 200, 400 and 800 years are displayed in Fig. 6. Fig. 6a shows the evolution in time of pore relative humidity profiles. The diffusion is so slow that even after eight centuries the pore humidity is far from uniform. The relative carbonation, $\mathcal{R}$, also proceeds very slowly, as confirmed by the curves in Fig. 6b. This small thickness, together with a nearly step-function profile of carbonation at the front, is why a uniform fine mesh was used (Fig. 5). Finally, Fig. 6c gives carbon dioxide concentration profiles. As the thickness of the cladding is the same for all the walls, the shape of these profiles varies with the depth of penetration beyond the cladding.

Regarding pore humidity, Fig. 7 shows the profiles computed for $t=800$ years, for walls of thicknesses $D=1.4$, 2.8, 5.6 m. The thin wall is almost dry whereas the thick wall is still humid. The difference is self-evident in the profiles of relative carbonation $\mathcal{R}$ presented in Fig. 8: the thin wall is fully carbonated whereas the thick wall is only partially carbonated. Space–time interaction maps better document the differences between thin and thick walls.

7. Space–time interaction maps

When dealing with time scales spanning many orders of magnitude, most of the transition from the initial value to the final asymptotic value occurs, in many diffusion and reaction problems, within only one or two orders of magnitude. To delimit the unreacted and reacted states, the transition may be considered to occur instantaneously at time τ_{sh}, called the half-time of the process, which is the time at which one half of the change from the initial to the final state has taken place. Thus the response may be approximated by a Heaviside step function of time having a step at τ_{sh}, which is shown for $\mathcal{R}$ in Fig. 9. In the sense of such Heaviside approximation, it becomes straightforward to separate the reacted and unreacted zones. The interaction map represents, for a certain value of $\sqrt{t}$, the location of the line separating the zone where the reaction degree reaches a specified percentage (such as 50%) of the transition from the initial to the final state.

In a linear problem of drying, the penetration front advances as $\sqrt{t}$ and initially this is also true for the total moisture loss from the specimen. Therefore, it is convenient to plot the space–time interaction maps in terms of $\sqrt{t}$ rather than t. Fig. 10 shows the interaction maps for both humidity ($h=0.85$, 0.9) and carbonation ($\mathcal{R}=0.9$). The bilinear trend is caused by the difference in diffusivity between the cladding and the core (with uniform diffusivity, a linear trend would occur).

Time curves (Fig. 9) and interaction maps (Fig. 10) show that carbonation starts when a certain threshold value of humidity is reached. This can be explained by observing that while pore humidity h remains high, coefficient $F_1(h)=(1-h)^{2.5}$ cuts down the diffusivity of carbon dioxide D_c, which is very small with respect to the diffusivity of relative pore humidity C. When the pore humidity drops below a certain value, coefficient D_c becomes several orders of magnitude higher than C. Now diffusion of carbon dioxide becomes sufficient to activate the reaction of carbonation, which is orders of magnitude faster than moisture diffusion in the thick wall.

The expression of $F_1(h)$, which is crucial for the carbonation progress [29], is still debated and researchers [20,22,29] proposed several equations. For this reason, a sound calibration based on comprehensive experiments on ancient lime concrete is advisable.

8. Sensitivity to main parameters

The expression of $F_1(h)$ is only one of the sources of uncertainty. Some authors have the opinion that humidity diffusion in ancient walls cannot be treated the same way as low strength Portland cement concrete. In ancient walls, due to the technique and the lack of vibration, large voids with very few connections can be found. Moreover, the construction by regular layers of bricks and pebbles alternated by thick layers of mortar (Fig. 1b) may introduce an orthotropic diffusivity. Diffusivity has been

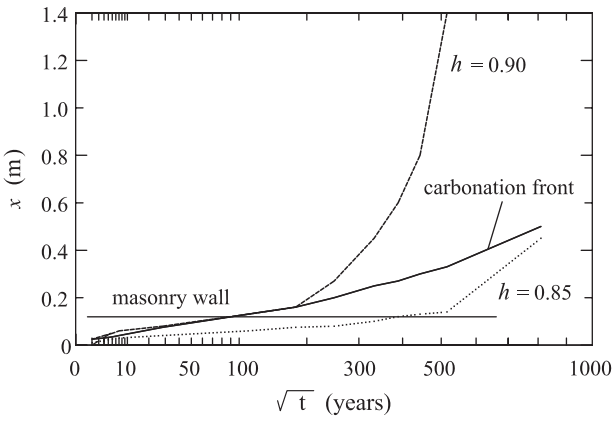

Fig. 10. Space–time interaction maps for humidity and carbonation.

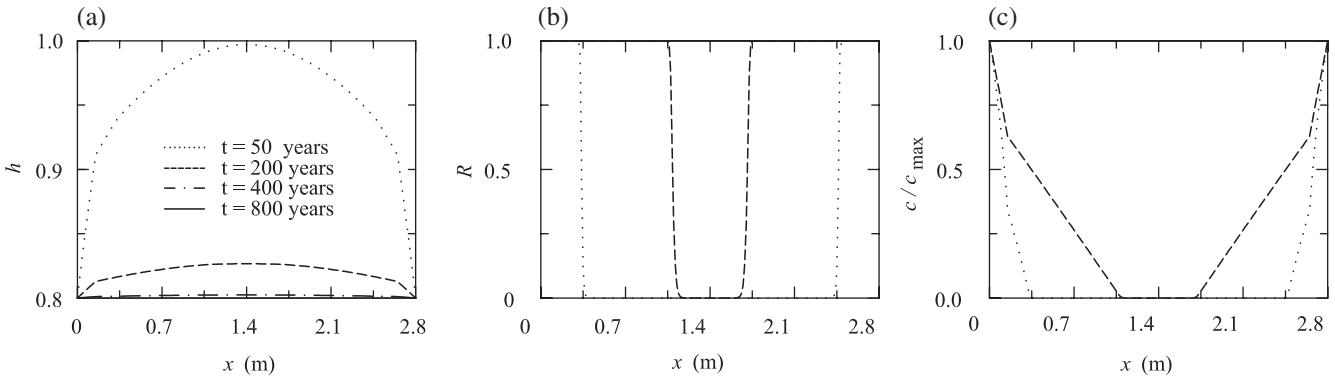

Fig. 11. Sensitivity to diffusion coefficients ($10C$, $10D_c$): (a) relative pore humidity h, (b) relative carbonation $\mathcal{R}$, (c) relative carbon dioxide concentration c/c_{max}.

studied far less for ancient walls than for Portland cement concrete and further research is needed. Until this is done, the assumption of a diffusivity similar to low strength Portland cement concrete gives the best possible estimate.

To examine the sensitivity of the solution to the value of diffusivity, the computations are repeated assuming higher and lower diffusivities, which may be associated with different porosities of the material. Fig. 11 shows the results for a wall of thickness $D=2.8$ m, obtained with diffusivities C and D_c replaced by $10C$ and $10D_c$. In this case, the wall, though massive, would dry almost completely after two centuries (Fig. 11a) and it would also completely carbonate after few years (Fig. 11b). Such behavior could not explain uncarbonated zones in some ancient walls.

On the contrary, with diffusivities C and D_c replaced by $0.1C$ and $0.1D_c$, the humidity in the core of the wall is still close to the initial value (Fig. 12a) and the carbonated region is only a few centimeters thick (Fig. 12b), in clear disagreement with the experimental evidence [41].

These limiting results appear to confirm that the orders of magnitude of the assumed parameters are correct. As pointed out in [41], some investigators have the opinion that most ancient lime mortar walls have reached complete carbonation. However, other researchers found uncarbonated lime mortar in very thick walls, especially in humid environment. This point is, of course, still debatable and will necessitate further research.

If observation on the presence and thickness of uncarbonated layers in thick walls was available, it could be used for a sound calibration of the coefficients of diffusion.

9. Closing comments

Moisture diffusion in ancient multiple-leaf masonry walls influences carbonation, shrinkage, creep and microcracking. These phenomena modify the mechanical behavior of the masonry in time producing a redistribution of stresses from the concrete core to the external layer, which is likely one of the causes of damage of some ancient towers. With these motivations, the interaction between moisture diffusion, carbon dioxide diffusion and carbonation has been modeled. Due to the absence of models and data for lime mortar, one of the simplest models proposed for Portland cement concrete was used [26]. The numerical results confirm that the time scale of the diffusion-reaction phenomena is compatible with the age at which some towers had problems. The time scale depends on the size of the walls and so walls of different thicknesses show different responses. Although based on typical parameters for Portland cement concrete, the results obtained seem realistic. The problem is clarified by introducing a mathematical approach into a subject in which disagreement has been largely due to qualitative nature of the previous studies. Once the experimental database is obtained, the model can be refined and recalibrated.

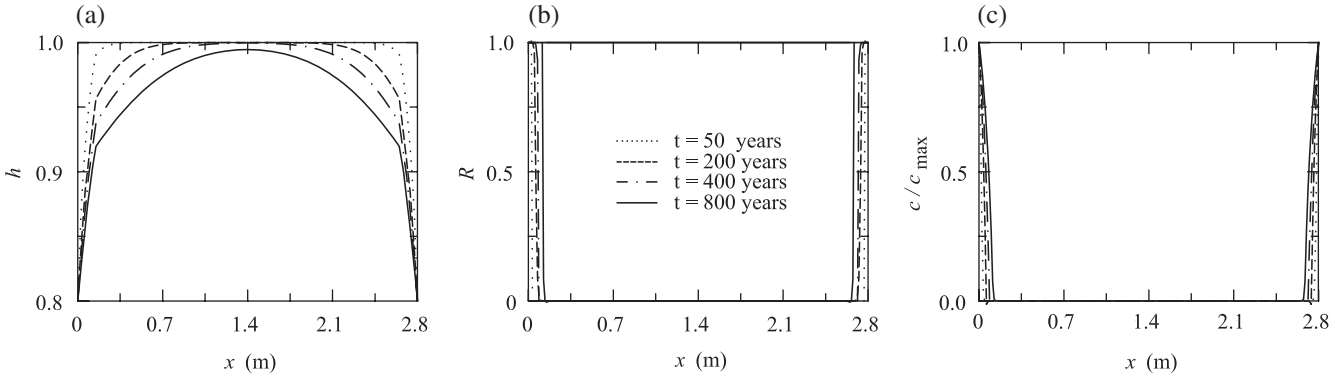

Fig. 12. Sensitivity to diffusion coefficients ($0.1C$, $0.1D_c$): (a) relative pore humidity h, (b) relative carbonation $\mathcal{R}$, (c) relative carbon dioxide concentration c/c_{max}.

Acknowledgment

Partial financial support from the U.S. National Science Foundation under grant CMS-0301145 is gratefully acknowledged.

References

[1] E. Heinle, F. Leonhardt, Towers: A Historical Survey, Rizzoli, New York, 1989.
[2] J. Heyman, Leaning towers, Meccanica 27 (3) (1992) 153–159.
[3] G. Croci, The conservation and structural restoration of architectural heritage, Advances in Architecture, vol. 1, Computational Mechanics Publications, Southampton, UK, 1998.
[4] G.M. Calvi, M.J.N. Priestley, Post collapse analyses of a medieval masonry tower, in: D. Abrams (Ed.), 5th North American Masonry Conference, Univ. of Illinois, Urbana-Champaign, Illinois, 1990, pp. 713–722.
[5] L. Binda, G. Gatti, G. Mangano, C. Poggi, G. Sacchi Landriani, The collapse of the civic tower of Pavia: a survey of the materials and structure, Mason. Int. 6 (1992) 11–20.
[6] A. Anzani, L. Binda, G. Melchiorri, Time dependent damage of rubble masonry walls, in: H. West (Ed.), 4th International Masonry Conference, British Masonry Society, London, 1995, pp. 341–351.
[7] A. Anzani, L. Binda, G. Mirabella Roberti, The effect of heavy persistent actions into the behaviour of ancient masonry, Mat. Struct., RILEM 33 (228) (2000) 251–261.
[8] E. Papa, A. Taliercio, L. Binda, Safety assessment of ancient masonry towers, in: B.H.V. Topping, C.A. Mota Soares (Eds.), 2nd Int. Congr. Studies in Ancient Structures, Vol. 1, Istanbul, Turkey, 2001, pp. 345–354.
[9] E. Papa, A. Taliercio, Prediction of the evolution of damage in ancient masonry towers, in: I. Mungan (Ed.), Int. Ass. for Shell and Spatial Structures IASS-MSU Int. Symp. Bridging Large Spans from Antiquity to the Present, Istanbul, Turkey, 2000, pp. 135–144.
[10] P. Bažant, T.-S. Wang, Practical prediction of cyclic humidity effect in creep and shrinkage, Mat. Struct., RILEM 18 (106) (1985) 247–252.
[11] M. Froli, P. Formichi, Statistical analysis of temperature measurements in the Leaning Tower of Pisa in comparison with theoretical predictions, Bautechnik 79 (10) (2002) 691–696.
[12] S.C. Anand, M.A. Rahman, Numerical modeling of creep in composite masonry walls, J. Struct. Eng., ASCE 117 (7) (1991) 2149–2165.
[13] Z.P. Bažant, D. Ferretti, Asymptotic temporal and spatial scaling of coupled creep, aging, diffusion and fracture, in: F.-J. Ulm, Z. Bažant, F. Wittmann (Eds.), Creep, Shrinkage and Durability Mechanics of Concrete and other Quasi-Brittle Materials, CONCREEP-6, Elsevier, Oxford, UK, 2001, pp. 121–145.
[14] Z.P. Bažant, J. Planas, Fracture and Size Effect in Concrete and Other Quasibrittle Materials, CRC Press, Boca Raton, 1998.
[15] Z.P. Bažant, Scaling of Structural Strength, Hermes Penton Science Publications, London, 2002.
[16] Z.P. Bažant, Scaling theory for quasibrittle structural failure, Proc. Natl. Acad. Sci. 101 (37) (2004) 13397–13399.
[17] D. Ferretti, I. Iori, G. Rizzi, The role of size effect in compression failure of ancient towers, in: G. Croci (Ed.), More than Two Thousand Years in the History of Architecture, International Council on Monuments and Sites ICOMOS-UNESCO, Paris, 2000, p. Ib 15.
[18] Z.P. Bažant, L.J. Najjar, Nonlinear water diffusion in nonsaturated concrete, Mat. Struct., RILEM 5 (25) (1972) 3–20.
[19] Z.P. Bažant, W.J. Raftshol, Effect of cracking in drying and shrinkage specimens, Cem. Concr. Res. 12 (2) (1982) 209–226 (disc. 797–798).
[20] K. van Balen, D. van Gemert, Modelling lime mortar carbonation, Mat. Struct., RILEM 27 (171) (1994) 393–398.
[21] D.R. Moorehead, Cementation by the carbonation of hydrated lime, Cem. Concr. 16 (1986) 700–708.
[22] K. van Balen, Carbonation reaction of lime, kinetics at ambient temperature, Cem. Concr. Res. 35 (2005) 647–657.
[23] L. Brieger, F.H. Wittmann, Numerical simulation of carbonation of concrete, in: F. Wittmann (Ed.), Material and Science Restoration, Tech. Akad. Esslingen, Ostfildern, 1986.
[24] V.G. Papadakis, C.G. Vayenas, M.N. Fardis, Fundamental modeling and experimental investigation of concrete carbonation, ACI Mater. J. 88 (4) (1991) 363–373.
[25] V.G. Papadakis, C.G. Vayenas, M.N. Fardis, Physical and chemical characteristics affecting the durability of concrete, ACI Mater. J. 88 (2) (1991) 186–196.
[26] A.V. Saetta, B.A. Schrefler, R. Vitaliani, The carbonation of concrete and the mechanism of moisture, heat and carbon dioxide flow through porous materials, Cem. Concr. Res. 23 (4) (1993) 761–772.
[27] A.V. Saetta, B.A. Schrefler, R. Vitaliani, 2-D model for carbonation and moisture/heat flow in porous materials, Cem. Concr. Res. 25 (8) (1995) 1703–1712.
[28] A.V. Saetta, R. Vitaliani, Experimental investigation and numerical modeling of carbonation process in reinforced concrete structures: Part I. Theoretical formulation, Cem. Concr. Res. 34 (4) (2004) 571–579.
[29] A. Steffens, D. Dinkler, H. Ahrens, Modeling carbonation for corrosion risk prediction of concrete structures, Cem. Concr. Res. 32 (6) (2002) 935–941.
[30] K. Maekawa, T. Ishida, Modeling of structural performances under coupled environmental and weather actions, Mat. Struct., RILEM 35 (254) (2002) 591–602.
[31] B. Isgor, A.G. Razaqpur, Finite element modeling of coupled heat transfer, moisture transport and carbonation process in concrete structures, Cem. Concr. 26 (1) (2004) 57–73.
[32] V.G. Papadakis, M.N. Fardis, C.G. Vayenas, Effect of composition, environmental factors and cement-lime mortar coating on concrete carbonation, Mat. Struct., RILEM 25 (154) (1992) 293–304.
[33] F. Henkel, Studies regarding the absorption of carbon dioxide by mortars, Zem. -Kalk-Gyps 11 (8) (1955) 386–393 (In German).
[34] O. Cazalla, C. Rodriguez-Navarro, E. Sebastian, G. Cultrone, Ageing of lime putty: effects on traditional lime mortar carbonation, J. Am. Ceram. Soc. 83 (5) (2000) 1070–1076.
[35] L. Ying-yu, W. Qui-dong, The mechanism of carbonation of mortars and the dependence of carbonation on pore structure, in: J. Scanlon (Ed.), Concrete Durability, ACI SP-100, Am. Concrete Inst, Detroit, 1987, pp. 1915–1929.
[36] K.J. Bathe, Finite Element Procedures, 2nd Edition Prentice Hall, Englewood, 1996.
[37] L.F. Shampine, Numerical Solution of Ordinary Differential Equations, Chapman & Hall, New York, 1994.
[38] C. Groot, J. Larbi, The influence of water flow (reversal) on bond strength development in young masonry, Heron 44 (2) (1999) 63–78.
[39] C. Andrade, J. Sarría, C. Alonso, Relative humidity in the interior of concrete exposed to natural and artificial weathering, Cem. Concr. Res. 29 (1999) 1249–1259.
[40] J. Lanas, J.I. Alvarez, Masonry repair lime-based mortars: factors affecting the mechanical behavior, Cem. Concr. Res. 33 (2003) 1867–1876.
[41] J. Adams, D. Dollimore, D.L. Griffiths, Thermal analytical investigation of in dated mortars and plasters, Thermochim. Acta 324 (1998) 67–76.